JCI The Journal of Clinical Investigation

Geranylgeranyltransferase type I (GGTase-I) deficiency hyperactivates macrophages and induces erosive arthritis in mice

Omar M. Khan, … , Maria Bokarewa, Martin O. Bergo

J Clin Invest. 2011;121(2):628-639. https://doi.org/10.1172/JCI43758.

Research Article

RHO family proteins are important for the function of inflammatory cells. They are modified with a 20-carbon geranylgeranyl lipid in a process catalyzed by protein geranylgeranyltransferase type I (GGTase-I). Geranylgeranylation is viewed as essential for the membrane targeting and activity of RHO proteins. Consequently, inhibiting GGTase-I to interfere with RHO protein activity has been proposed as a strategy to treat inflammatory disorders. However, here we show that mice lacking GGTase-I in macrophages develop severe joint inflammation resembling erosive rheumatoid arthritis. The disease was initiated by the GGTase-I–deficient macrophages and was transplantable and reversible in bone marrow transplantation experiments. The cells accumulated high levels of active GTP-bound RAC1, CDC42, and RHOA, and RAC1 remained associated with the plasma membrane. Moreover, GGTase-I deficiency activated p38 and NF-κB and increased the production of proinflammatory cytokines. The results challenge the view that geranylgeranylation is essential for the activity and localization of RHO family proteins and suggest that reduced geranylgeranylation in macrophages can initiate erosive arthritis.

 Related Commentary, page 510

Geranylgeranyltransferase type I (GGTase-I) deficiency hyperactivates macrophages and induces erosive arthritis in mice

Omar M. Khan,[1] Mohamed X. Ibrahim,[1] Ing-Marie Jonsson,[2] Christin Karlsson,[1] Meng Liu,[1,3] Anna-Karin M. Sjogren,[1] Frida J. Olofsson,[1] Mikael Brisslert,[2] Sofia Andersson,[2] Claes Ohlsson,[4] Lillemor Mattsson Hultén,[1] Maria Bokarewa,[2] and Martin O. Bergo[1]

[1]Sahlgrenska Center for Cardiovascular and Metabolic Research, Wallenberg Laboratory, Department of Molecular and Clinical Medicine, and [2]Department of Rheumatology, Institute of Medicine, Sahlgrenska Academy, University of Gothenburg, Gothenburg, Sweden. [3]Department of Neurosurgery, Qilu Hospital, Shandong University, Jinan, China. [4]Department of Internal Medicine, Institute of Medicine, Sahlgrenska Academy, University of Gothenburg, Gothenburg, Sweden.

RHO family proteins are important for the function of inflammatory cells. They are modified with a 20-carbon geranylgeranyl lipid in a process catalyzed by protein geranylgeranyltransferase type I (GGTase-I). Geranylgeranylation is viewed as essential for the membrane targeting and activity of RHO proteins. Consequently, inhibiting GGTase-I to interfere with RHO protein activity has been proposed as a strategy to treat inflammatory disorders. However, here we show that mice lacking GGTase-I in macrophages develop severe joint inflammation resembling erosive rheumatoid arthritis. The disease was initiated by the GGTase-I–deficient macrophages and was transplantable and reversible in bone marrow transplantation experiments. The cells accumulated high levels of active GTP-bound RAC1, CDC42, and RHOA, and RAC1 remained associated with the plasma membrane. Moreover, GGTase-I deficiency activated p38 and NF-κB and increased the production of proinflammatory cytokines. The results challenge the view that geranylgeranylation is essential for the activity and localization of RHO family proteins and suggest that reduced geranylgeranylation in macrophages can initiate erosive arthritis.

Introduction

Small GTPases of RHO family proteins such as RAC1, RHOA, and CDC42 regulate the actin cytoskeleton during cell migration and phagocytosis and participate in intracellular signaling pathways (1, 2). RHO family proteins are modified with a 20-carbon geranylgeranyl lipid on the cysteine residue of a carboxyterminal *CAAX* motif, a modification catalyzed by protein geranylgeranyltransferase type I (GGTase-I) (3). Other *CAAX* proteins, such as RAS and prelamin A, are modified with a 15-carbon farnesyl lipid by farnesyltransferase (FTase). Farnesylation and geranylgeranylation are collectively called prenylation. GGTase-I and FTase are cytosolic enzymes that share a common α subunit but have distinct β subunits that dictate substrate specificity (3).

Geranylgeranylation facilitates membrane anchoring and is considered essential for the subcellular targeting and activation of RHO family proteins (4, 5). For example, when the geranylgeranyl cysteine residue of RAC1 is clipped off by the bacterial YopT protease or when the cysteine in its *CAAX* motif is mutated to serine, RAC1 localizes to the nucleus (6–8). Geranylgeranylation may also be important for protein–protein interactions, such as the binding of RHO proteins to RHO GTPase activating proteins (RHO-GAPs), which stimulate GTP hydrolysis and inactivation; RHO guanine nucleotide exchange factors (RHO-GEFs), which stimulate GDP/GTP exchange and activation; and RHO guanine-nucleotide dissociation inhibitor (RHO-GDI), which sequesters the GDP-bound inactive form of RHO proteins in the cytosol (8–11). Thus, inhibiting the geranylgeranylation of RHO family proteins might interfere with their targeting to membranes and their function.

GGTase-I inhibitors (GGTIs) were developed as anticancer drugs primarily because several RHO family members contribute to tumor growth and metastasis (12). GGTase-I was validated as a drug target with genetic strategies in mice (13), and one GGTI is being evaluated in a phase I clinical trial. But the activities of RHO family proteins are also important for the ability of macrophages and lymphocytes to migrate into tissues, respond to inflammatory stimuli, and trigger ROS production, phagocytosis, NF-κB signaling, and cytokine production (2). Consequently, inhibiting GGTase-I has been viewed as a potential strategy to inhibit the proinflammatory activities of RHO family proteins and to treat inflammatory and autoimmune diseases such as rheumatoid arthritis (14, 15).

Inhibiting the geranylgeranylation of RHO family proteins has also been proposed to explain the antiinflammatory properties and other pleiotropic effects of statins (16, 17). These widely used cholesterol-lowering drugs may be beneficial in the treatment of rheumatoid arthritis and autoimmune diseases (17–20). Statins lower cholesterol levels by blocking the production of mevalonate, which reduces the levels of geranylgeranyl pyrophosphate, the lipid substrate for GGTase-I, and, to a lesser extent, the levels of farnesyl pyrophosphate, the lipid substrate for FTase (21).

Thus, several lines of investigation suggest that inhibiting protein geranylgeranylation might be a strategy to treat inflammatory diseases, but to our knowledge, the effects of inhibiting GGTase-I have not been convincingly assessed in mouse models of inflammation. To address this issue, we bred conditional GGTase-I knockout mice with mice expressing Cre recombinase in macrophages, with the goal of defining how GGTase-I deficiency affects

Conflict of interest: The authors have declared that no conflict of interest exists.
Citation for this article: *J Clin Invest.* 2011;121(2):628–639. doi:10.1172/JCI43758.

macrophage function in vitro and the development of inflammatory diseases in vivo. Surprisingly, GGTase-I deficiency did not impair macrophage migration or phagocytosis and resulted in accumulation of GTP-bound RAC1, increased production of ROS and proinflammatory cytokines, and progressive erosive arthritis.

Results

Inactivating GGTase-I in macrophages induces spontaneous erosive arthritis in mice. To produce mice lacking GGTase-I in macrophages, we used a conditional GGTase-I knockout allele (*Pggt1b*^{fl}) and a lysozyme M-*Cre* allele (*LC*) (13). The extent of Cre recombination of *Pggt1b* in BM-derived macrophages was greater than 90%, as judged by quantitative PCR (QPCR) of genomic DNA (Figure 1A), which suggests that the majority of macrophages lacked both copies of *Pggt1b*. Similarly, recombination in osteoclasts was 84%. In neutrophils, the extent of recombination of *Pggt1b* was 40%; recombination in dendritic cells and lymphocytes was low (Figure 1A). *Pggt1b*$^{fl/fl}$*LC* mice are born at Mendelian ratios and have no obvious phenotypes; the red and white blood cell counts and the percentages of monocytes, neutrophils, and lymphocytes in peripheral blood are unaffected (13).

Histological analyses of joints of 8- to 17-week-old *Pggt1b*$^{fl/fl}$*LC* mice revealed severe inflammation characterized by accumulation of leukocytes, proliferation of synovial tissue (synovitis), and bone erosions (Figure 1, B and C). The lesions were most pronounced in metatarsal and metacarpal joints but were also found in the ankle, wrist, knee, and elbow. Synovitis was mild, and no bone erosions were identified, in joints of 3-week-old *Pggt1b*$^{fl/fl}$*LC* mice (data not shown). The disease phenotypes were similar in *Pggt1b*$^{fl/fl}$*LC* mice maintained on mixed (129Sv/Ola-C57BL/6) and 5-generation inbred (C57BL/6) genetic backgrounds. Littermate *Pggt1b*$^{fl/+}$*LC* and wild-type control mice had normal joint histology, typically with a single-cell-layer synovium (Figure 1, B and C). Bone erosions in *Pggt1b*$^{fl/fl}$*LC* mice were visible on microcomputerized tomography scans of the knee, but the mineral density of trabecular and cortical bone and the cortical thickness of femur and tibia were not different in *Pggt1b*$^{fl/fl}$*LC* and *Pggt1b*$^{fl/+}$*LC* mice (Supplemental Figure 1, A–D; supplemental material available online with this article; doi:10.1172/JCI43758DS1). The *Pggt1b*$^{fl/fl}$*LC* mice had no histological evidence of inflammation in lung, liver, or kidneys (Supplemental Figure 1E).

To determine whether FTase deficiency in macrophages induces joint inflammation, we used a conditional allele for the FTase β subunit (*Fntb*^{fl}) (22) to produce *Fntb*$^{fl/fl}$*LC* mice. At 33 weeks of age, *Fntb*$^{fl/fl}$*LC* mice had no signs of inflammation and were indistinguishable from *Fntb*$^{fl/+}$*LC* and wild-type controls (Figure 1B). Moreover, simultaneous inactivation of FTase and GGTase-I (i.e., in *Pggt1b*$^{fl/fl}$*Fntb*$^{fl/fl}$*LC* mice) resulted in phenotypes similar to those after inactivation of GGTase-I alone (Figure 1B).

The arthritis in Pggt1b$^{fl/fl}$*LC mice is mediated by macrophages*. Immunohistochemical analysis of the thickened synovial lining in joints of *Pggt1b*$^{fl/fl}$*LC* mice revealed widespread staining of F4/80 (a marker of mature macrophages) and nonprenylated RAP1A (np-RAP1A; a marker of cells lacking GGTase-I) (22) and moderate staining of the T lymphocyte marker CD4 (Figure 1D). The specificity of the np-RAP1A antibody is illustrated in Supplemental Figure 1F.

To determine whether macrophages are a driving force in arthritis development, we injected 4-week-old *Pggt1b*$^{fl/fl}$*LC* mice with etoposide, which reduces levels of circulating monocytes by greater than 90% and has little effect on granulocytes and lymphocytes (23, 24). After 8 weeks of treatment, the mean synovitis score was reduced by 72%, and the mean bone erosion score was reduced by 35% (Figure 1E).

To assess inflammatory responses, *Pggt1b*$^{fl/fl}$*LC* and *Pggt1b*$^{fl/+}$*LC* mice were challenged with an olive oil injection in the hind paw to induce neutrophil-dependent inflammation or with an oxazolone-induced delayed-type hypersensitivity reaction to induce T lymphocyte–dependent inflammation. The responses of *Pggt1b*$^{fl/fl}$*LC* and *Pggt1b*$^{fl/+}$*LC* mice did not differ significantly (Supplemental Figure 1, G and H), consistent with the low level of *Pggt1b* knockout in those cell types (Figure 1A).

Evaluation of humoral responses revealed higher serum levels of autoantibodies recognizing citrullinated peptides (CCP), Fc chain of Igs (rheumatoid factor [RF]), and single-stranded DNA (ssDNA) in *Pggt1b*$^{fl/fl}$*LC* mice than in *Pggt1b*$^{fl/+}$*LC* mice (Figure 1F), which suggests that B lymphocytes are secondarily affected by GGTase-I deficiency in macrophages.

The erosive arthritis of Pggt1b$^{fl/fl}$*LC mice is transplantable and reversible*. To rule out mosaic expression of Cre in non-BM cell types as a cause of arthritis in *Pggt1b*$^{fl/fl}$*LC* mice, we performed BM transplantation experiments. *Pggt1b*$^{fl/fl}$*LC* BM cells stably repopulated lethally irradiated wild-type recipient mice and induced mild synovitis at 8 weeks and robust synovitis with bone erosions at 14 weeks after transplantation (Figure 1G and Supplemental Figure 2A). After transplantation of wild-type BM cells in 12-week-old *Pggt1b*$^{fl/fl}$*LC* mice, which invariably had severe disease phenotypes, joint inflammation and bone erosions were reduced at 8 weeks and largely eliminated at 14 weeks (Figure 1H and Supplemental Figure 2A). The improved arthritis phenotypes were likely not a result of irradiation per se, as lethally irradiated *Pggt1b*$^{fl/fl}$*LC* recipients of *Pggt1b*$^{fl/fl}$*LC* BM cells had levels of inflammation and erosion similar to those in untransplanted controls (Supplemental Figure 2B).

GGTase-I–deficient macrophages are small and rounded, but migration and phagocytosis are unaffected. We harvested BM cells from *Pggt1b*$^{fl/fl}$*LC* and *Pggt1b*$^{fl/+}$*LC* mice and differentiated them into macrophages in medium containing M-CSF. *Pggt1b*$^{fl/fl}$*LC* and *Pggt1b*$^{fl/+}$*LC* macrophages expressed similar levels of macrophage cell surface markers, as judged by fluorescence-activated cell sorting (FACS; Figure 2A). np-RAP1A accumulated in *Pggt1b*$^{fl/fl}$*LC* BM macrophages and in *Pggt1b*$^{fl/+}$*LC* BM macrophages incubated with a GGTI, as judged by Western blot of total cell lysates; np-RAP1A levels were low in *Pggt1b*$^{fl/fl}$*LC* BM macrophages incubated with a lentivirus expressing human *PGGT1B* (lenti-*PGGT1B*) and undetectable in *Pggt1b*$^{fl/+}$*LC* BM macrophages (Figure 2B).

Pggt1b$^{fl/fl}$*LC* BM macrophages were small and rounded, with an average cell adhesive area approximately 80% smaller than in *Pggt1b*$^{fl/+}$*LC* macrophages (Figure 2, C and D). This morphological phenotype was also observed in i.p. macrophages isolated from *Pggt1b*$^{fl/fl}$*LC* mice and in *Pggt1b*$^{fl/+}$*LC* BM and i.p. macrophages incubated with a GGTI (Figure 2C). Moreover, the adhesive area of *Pggt1b*$^{fl/fl}$*LC* BM macrophages increased after incubation with lenti-*PGGT1B* (Figure 2, C and D). Lentiviral expression of mutant RAC1 and RHOA engineered to undergo farnesylation by FTase (fRAC1 and fRHOA, respectively; Figure 2E) also increased the adhesive area of *Pggt1b*$^{fl/fl}$*LC* BM macrophages (Figure 2, C and D).

After 7 days in M-CSF culture, *Pggt1b*$^{fl/fl}$*LC* BM produced 30% fewer macrophages than *Pggt1b*$^{fl/+}$*LC* BM, but the number of apoptotic cells was not different (Figure 2, F and G). However, after i.p. injections of uric acid, similar numbers of macrophages were isolated from the abdominal cavity of *Pggt1b*$^{fl/fl}$*LC* and *Pggt1b*$^{fl/+}$*LC*

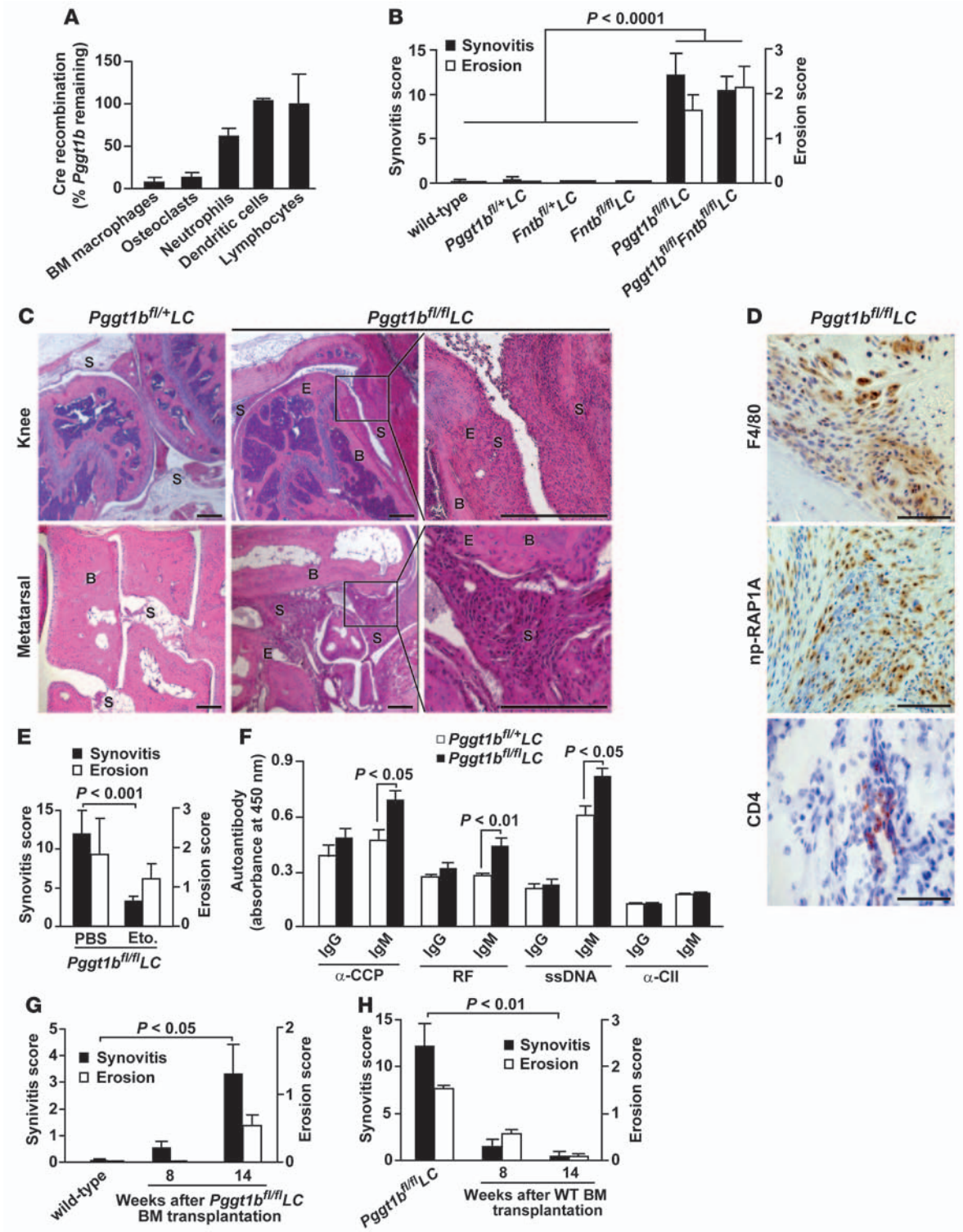
A
Cre recombination (% Pggt1b remaining)
150
100
50
0
BM macrophages
Osteoclasts
Neutrophils
Dendritic cells
Lymphocytes
B
P < 0.0001
Synovitis
Erosion
Synovitis score
Erosion score
wild-type
Pggt1b fl/+ LC
Fntb fl/+ LC
Fntb fl/fl LC
Pggt1b fl/fl LC
Pggt1b fl/fl Fntb fl/fl LC
C
Pggt1b fl/+ LC
Pggt1b fl/fl LC
Knee
Metatarsal
S
E
B
D
Pggt1b fl/fl LC
F4/80
np-RAP1A
CD4
E
Synovitis
Erosion
P < 0.001
Synovitis score
Erosion score
PBS
Eto.
Pggt1b fl/fl LC
F
Pggt1b fl/+ LC
Pggt1b fl/fl LC
Autoantibody (absorbance at 450 nm)
P < 0.05
P < 0.01
P < 0.05
IgG
IgM
α-CCP
RF
ssDNA
α-CII
G
P < 0.05
Synovitis
Erosion
Synivitis score
Erosion score
wild-type
8
14
Weeks after Pggt1b fl/fl LC BM transplantation
H
P < 0.01
Synovitis
Erosion
Synovitis score
Erosion score
Pggt1b fl/fl LC
8
14
Weeks after WT BM transplantation

Figure 1
Knockout of GGTase-I in macrophages induces erosive arthritis in mice. (**A**) QPCR showing Cre-induced recombination in genomic DNA of different cell types of *Pggt1b$^{fl/fl}$LC* mice (n = 2–3). (**B**) Synovitis and bone erosion in joints of 5- to 20-week-old wild-type (n = 5), 8- to 32-week-old *Pggt1b$^{fl/+}$LC* (n = 15), 33-week-old *Fntb$^{fl/+}$LC* and *Fntb$^{fl/fl}$LC* (n = 3), 8- to 17-week-old *Pggt1b$^{fl/fl}$LC* (n = 10), and 20- to 30-week-old *Pggt1b$^{fl/fl}$Fntb$^{fl/fl}$LC* (n = 9) mice. (**C**) Hematoxylin and eosin–stained sections of joints from 12-week-old mice. S, synovium; B, bone; E, erosion. Scale bars: 400 μm (top); 200 μm (bottom). (**D**) Immunohistochemical staining of the thickened synovial lining in the knee of a 12-week-old *Pggt1b$^{fl/fl}$LC* mouse to visualize macrophages (F4/80), cells lacking GGTase-I (np-RAP1A), and T lymphocytes (CD4). Scale bars: 100 μm. (**E**) Synovitis and bone erosion in joints of 12-week-old *Pggt1b$^{fl/fl}$LC* mice injected with etoposide (10 mg/kg s.c., n = 14) or vehicle (PBS, n = 6) for 8 weeks. (**F**) Levels of autoantibodies in serum of 8- to 12-week-old *Pggt1b$^{fl/+}$LC* and *Pggt1b$^{fl/fl}$LC* mice (n = 14–20 per genotype). CII, collagen type II. (**G**) Synovitis and bone erosion in joints of wild-type control mice and 2 groups of wild-type mice (n = 9–10 per group) irradiated at 8 weeks of age and transplanted with BM cells from *Pggt1b$^{fl/fl}$LC* mice. (**H**) Synovitis and bone erosion in *Pggt1b$^{fl/fl}$LC* mice and 2 groups of *Pggt1b$^{fl/fl}$LC* mice (n = 6 per group) irradiated at 12 weeks of age and transplanted with BM from wild-type mice.

mice (Figure 2H). Despite the striking morphological phenotype of *Pggt1b$^{fl/fl}$LC* BM macrophages, their ability to phagocytose and kill bacteria and to migrate in response to D-peptide, a potent chemotactic agent, was similar to that of *Pggt1b$^{fl/+}$LC* macrophages (Figure 2, I and J). Similar results were obtained with i.p. macrophages (data not shown).

RHO proteins accumulate in GTP-bound form, and RAC1 remains associated with the plasma membrane, in GGTase-I–deficient macrophages. We found a striking accumulation of GTP-bound RAC1 in *Pggt1b$^{fl/fl}$LC* macrophages, as shown by affinity precipitation and Western blots of lysates (Figure 3A). RAC1 in *Pggt1b$^{fl/fl}$LC* and *Pggt1b$^{fl/+}$LC* macrophages incubated with a GGTI had reduced electrophoretic mobility, characteristic of the nonprenylated form of the protein (Figure 3A and Supplemental Figure 3, A and B). RAC1 was undetectable in lysates of *Rac1*-deficient fibroblasts, documenting the specificity of the antibody (Supplemental Figure 3C). GTP-bound CDC42 and RHOA also accumulated in *Pggt1b$^{fl/fl}$LC* macrophages (Figure 3, B and C). Total levels of RAC1 and CDC42 were similar in *Pggt1b$^{fl/fl}$LC* and *Pggt1b$^{fl/+}$LC* cells; total levels of RHOA were slightly increased (Figure 3, A–C).

From previous studies, we suspected that nonprenylated RAC1 would accumulate in the nucleus (6–8). This suspicion was not upheld. Western blots of subcellular fractions of *Pggt1b$^{fl/fl}$LC* macrophages revealed RAC1 in the membrane and cytosolic fractions, as in *Pggt1b$^{fl/+}$LC* macrophages, which had trace amounts of nuclear RAC1 (Figure 3D). RHOA and CDC42 were mainly cytosolic in both *Pggt1b$^{fl/fl}$LC* and *Pggt1b$^{fl/+}$LC* macrophages, although the latter cells had trace amounts in the membrane fraction (Figure 3D).

In *Pggt1b$^{fl/+}$LC* macrophages, RAC1 was associated with the endoplasmic reticulum and the plasma membrane, including clear staining at membrane ruffles and filopodia, as shown by immunofluorescence confocal microscopy (Figure 3E). RAC1 immunostaining was reduced by treatment with a *RAC1* shRNA lentivirus, but not a *RAC2* shRNA lentivirus, demonstrating the specificity of the antibody (Supplemental Figure 3D). In *Pggt1b$^{fl/fl}$LC* macrophages, RAC1 staining was observed at perinuclear structures, was clearly localized at the plasma membrane, and overlapped considerably with staining of the plasma membrane protein Na/K-ATPase (Figure 3E). Incubating *Pggt1b$^{fl/fl}$LC* and *Pggt1b$^{fl/+}$LC* macrophages with an FTI and a GGTI did not affect RAC1 plasma membrane localization (Supplemental Figure 3E).

Immunoprecipitation and Western blot analyses revealed less association of RHO-GDI with RAC1 and CDC42 in *Pggt1b$^{fl/fl}$LC* than in *Pggt1b$^{fl/+}$LC* macrophages (Figure 3F). The association of RHO-GDI with RHOA was unaffected by GGTase-I deficiency (Figure 3F).

RHO family proteins accumulate in unprocessed form in GGTase-I–deficient macrophages. To determine whether GGTase-I substrates accumulate in unprocessed form in GGTase-I–deficient macrophages, we incubated whole-cell lysates of *Pggt1b$^{fl/fl}$LC* and *Pggt1b$^{fl/+}$LC* macrophages with ^{3}H-GGPP and recombinant human GGTase-I. In this assay, ^{3}H-GGPP was readily incorporated into unprocessed substrates by recombinant GGTase-I in vitro; total proteins or RAC1 and RHOA immunoprecipitated from the reaction mixture were resolved by SDS-PAGE and visualized by autoradiography. As expected, no ^{3}H-GGPP was incorporated into proteins in *Pggt1b$^{fl/+}$LC* extracts (Figure 3G), which indicated that all GGTase-I substrates had already been prenylated by endogenous GGTase-I. In contrast, there was robust incorporation of ^{3}H-GGPP into total proteins, RAC1, and RHOA in *Pggt1b$^{fl/fl}$LC* extracts (Figure 3G). Thus, RHO family proteins accumulate in unprocessed form in *Pggt1b$^{fl/fl}$LC* cells.

Knockout of GGTase-I activates proinflammatory signaling pathways. Next, we determined whether RAC1-GTP accumulation in GGTase-I–deficient macrophages increases ROS production and other pathways downstream of RAC1. First, we stimulated the cells with PMA. ROS production was greater in *Pggt1b$^{fl/fl}$LC* than in *Pggt1b$^{fl/+}$LC* macrophages (Figure 4A). Second, we performed Western blots on lysates of *Pggt1b$^{fl/fl}$LC* and *Pggt1b$^{fl/+}$LC* macrophages before and after LPS stimulation. LPS-stimulated phosphorylation of p38 was increased in *Pggt1b$^{fl/fl}$LC* macrophages (Figure 4B). Finally, LPS-induced phosphorylation and DNA-binding activity of the NF-κB p65 subunit were higher in *Pggt1b$^{fl/fl}$LC* macrophages (Figure 4, C and D).

Consistent with increased NF-κB activation, expression of *Csf2*, *Tnfa*, *Il1b*, *Il6*, and 8 other NF-κB–regulated genes was higher, and expression of 3 such genes was lower, in LPS-stimulated *Pggt1b$^{fl/fl}$LC* than in *Pggt1b$^{fl/+}$LC* BM macrophages (Figure 4E, Supplemental Figure 4A, and Supplemental Table 1). Expression of *Adamts1*, fibronectin (*Fn1*), *Mmp3*, *Mmp12*, and genes encoding 4 other extracellular matrix–associated proteins was also increased (Figure 4F and Supplemental Table 2). Similar gene expression changes were observed in i.p. macrophages (Supplemental Figure 4B). Moreover, the medium of LPS-stimulated *Pggt1b$^{fl/fl}$LC* macrophages contained higher concentrations of TNF-α, IL-1β, and IL-6 (Figure 4G) as well as interferon-γ, IL-10, IL-12p70, and KC (data not shown). We also observed increased secretion of cytokines in *Pggt1b$^{fl/+}$LC* macrophages incubated with a GGTI before and during LPS stimulation (Figure 4G).

Inhibiting RAC1 reduces cytokine production of macrophages in vitro, and TNF-α inhibition reduces joint inflammation in vivo. To assess the role of RAC1 in the increased cytokine production of *Pggt1b$^{fl/fl}$LC* BM macrophages, we incubated the cells with lentiviral constructs before and during LPS stimulation and measured IL-1β levels in the medium. As expected, IL-1β levels were reduced by lenti-*PGGT1B* but were unaffected by expression of fRAC1 or fRHOA; IL-1β levels were also markedly reduced by knockdown of *RAC1*

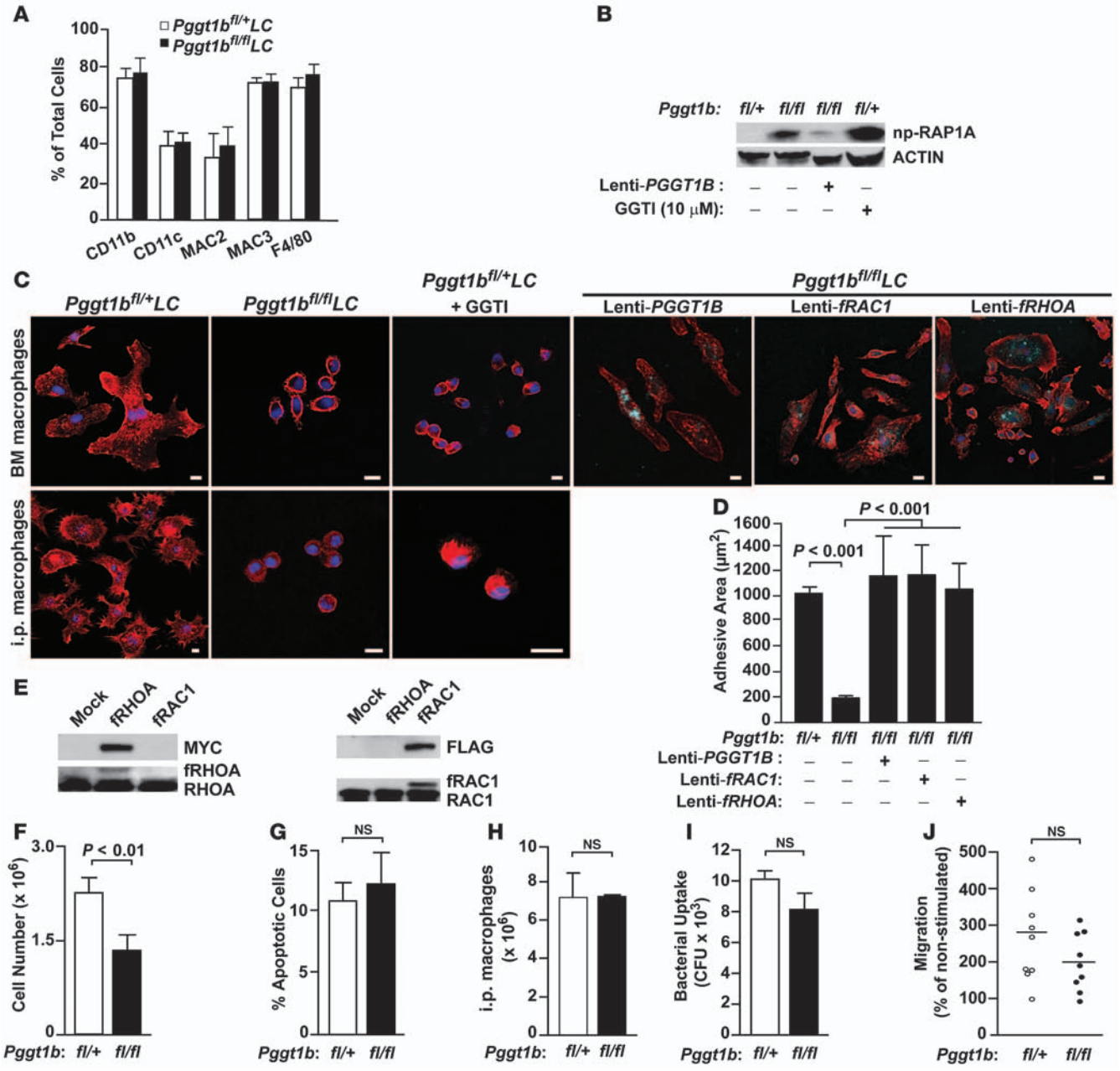

Figure 2

GGTase-I–deficient macrophages have smaller adhesive area, but no defects in phagocytosis and migration. (**A**) FACS analyses of BM macrophages with antibodies against macrophage surface markers (n = 5 per genotype). (**B**) Western blot of BM macrophage lysates revealed low levels of np-RAP1A in *Pggt1b$^{fl/+}$LC* cells and *Pggt1b$^{fl/fl}$LC* cells incubated for 2 days with lenti-*PGGT1B*, and high levels in untreated *Pggt1b$^{fl/fl}$LC* cells and *Pggt1b$^{fl/+}$LC* cells incubated for 12 hours with a GGTI (GGTI-298; 10 μM). Actin was used as loading control. (**C**) Confocal micrographs of phalloidin-stained (red) untreated macrophages, and macrophages treated for 12 hours with GGTI-298 (10 μM) or lentiviruses expressing dTomato (blue) and either PGGT1B, fRAC1, or fRHOA. Scale bars: 10 μm. (**D**) Adhesive area of untreated and dTomato-positive macrophages expressing PGGT1B, fRAC1, or fRHOA (n = 3–5 per genotype). (**E**) Western blot of lysates from lentivirus-treated fibroblasts showing expression of fRHOA (MYC-tagged) and fRAC1 (FLAG-tagged). Identical blots were probed with antibodies recognizing endogenous RHOA and RAC1 and the slower migrating recombinant proteins. (**F**) Number of BM-derived macrophages after 7 days in M-CSF culture (n = 6 per genotype). (**G**) FACS analyses with EGFP–annexin V to detect apoptotic macrophages from the experiment in **F** (n = 3 per genotype). (**H**) Number of i.p. macrophages isolated from mice 4 days after i.p. injection of uric acid (n = 3 per genotype). (**I**) Phagocytosis of BM macrophages, expressed as CFU of phagocytosed bacteria (n = 5 per genotype). (**J**) D-peptide–stimulated migration of BM macrophages (n = 9 per genotype).

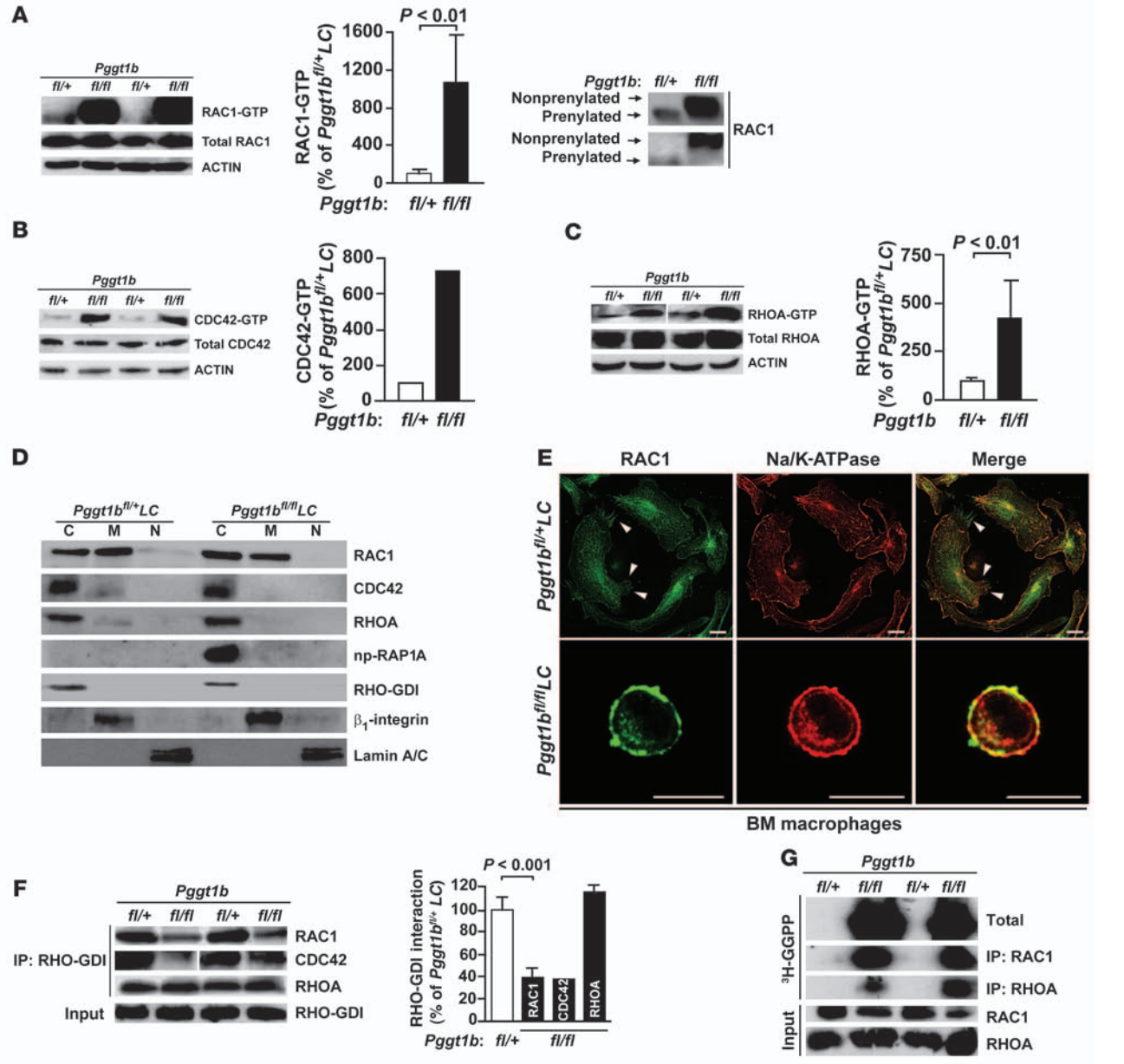

Figure 3

Knockout of GGTase-I results in accumulation of GTP-bound RHO family proteins and has little effect on the subcellular localization of RAC1. (**A**–**C**) Western blots show levels of GTP-bound and total RAC1 (**A**), CDC42 (**B**), and RHOA (**C**) in lysates from BM macrophages. Actin was used as a loading control. Corresponding graphs show the amount of GTP-bound RAC1 ($n = 7$), CDC42 ($n = 2$), and RHOA ($n = 4$) determined by densitometry. Reduced electrophoretic mobility of affinity-purified RAC1 in lysates from *Pggt1b*$^{fl/fl}$*LC* macrophages (run on 12% Protean gels) is also shown in **A**. (**D**) Western blots showing the distribution of RAC1, CDC42, RHOA, and np-RAP1A in the cytosol (C), membrane (M), and nuclear (N) fractions of BM macrophages. RHO-GDI, β_1-integrin, and lamin A/C were used as markers for cytosol, membrane, and nuclear fractions, respectively. (**E**) Confocal micrographs showing immunohistochemical staining of BM macrophages with antibodies against RAC1 and Na/K-ATPase. Arrowheads indicate RAC1 at filopodia at the plasma membrane. Scale bars: 10 μm. (**F**) Immunoprecipitation of RHO-GDI in lysates of BM macrophages followed by Western blot for RAC1, CDC42, and RHOA. Levels of RHO-GDI–bound RAC1 ($n = 4$), CDC42 ($n = 2$), and RHOA ($n = 4$), as determined by densitometry, are also shown. Lanes were run on the same gel but were noncontiguous (white line). (**G**) Accumulation of unprocessed GGTase-I substrates susceptible to in vitro prenylation by ^{3}H-GGPP and recombinant GGTase-I. The experiment was repeated twice with similar results.

with a *RAC1* shRNA lentivirus but were unaffected by *RAC2* or sequence-scrambled shRNA (Figure 5A). The shRNAs reduced expression by 60%–90%, as determined by semiquantitative RT-PCR (Figure 5B) and TaqMan RT-QPCR (data not shown). IL-1β and TNF-α levels were reduced in a dose-dependent fashion in the medium of *Pggt1b*$^{fl/fl}$*LC* macrophages incubated with a RAC1 inhibitor and an inhibitor of the RAC1 downstream effector PAK (Figure 5, C and D). Thus, the high levels of RAC1-GTP in GGTase-I–deficient macrophages likely caused the increased IL-1β and TNF-α production.

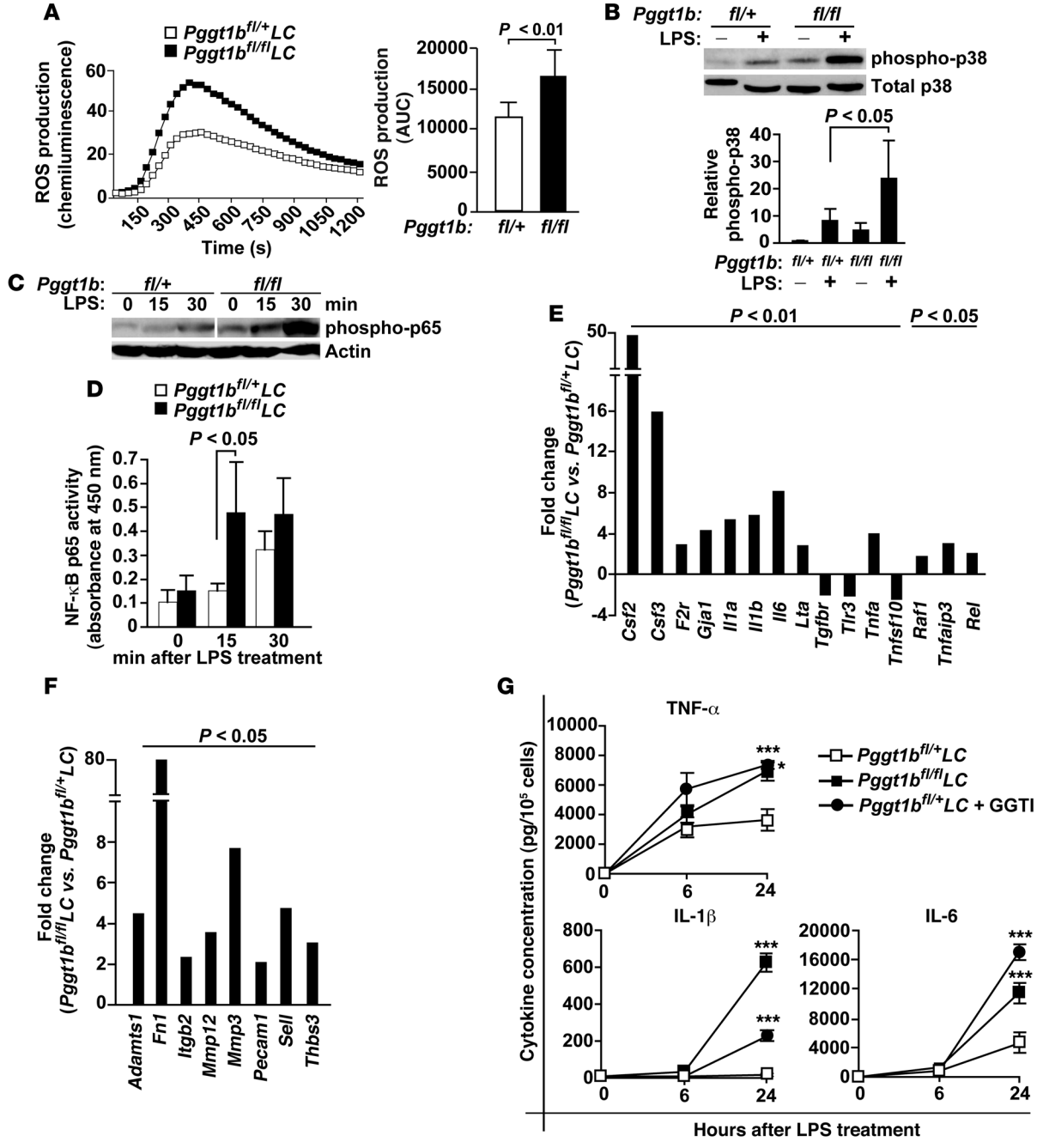

Figure 4

GGTase-I–deficient macrophages exhibit increased activation of proinflammatory signaling pathways. (**A**) ROS production was measured in real time after stimulation of BM macrophages with 50 μM PMA. Total ROS production in BM macrophages is also shown (n = 11 per genotype). (**B**) Western blots of lysates from BM macrophages showing basal and LPS-stimulated p38 phosphorylation. Also shown are levels of phospho-p38 as determined by densitometry, expressed relative to unstimulated *Pggt1b*$^{fl/+}$*LC* BM macrophages (n = 5 per genotype). (**C**) Western blot of lysates from basal and LPS-stimulated BM macrophages with an antibody to phospho-p65 subunit of NF-κB. Actin was used as a loading control. Lanes were run on the same gel but were noncontiguous (white line). (**D**) NF-κB p65 activity assay of lysates of BM macrophages (n = 5 per genotype). (**E**) Data from low-density QPCR array showing the relative change in expression of 15 NF-κB–regulated genes in LPS-stimulated *Pggt1b*$^{fl/fl}$*LC* compared with *Pggt1b*$^{fl/+}$*LC* BM macrophages (n = 6 per genotype). (**F**) Data from low-density QPCR array using the same cDNA as in **E**, showing the relative change in expression of 8 genes involved in extracellular matrix remodeling and cell adhesion (n = 6 per genotype). Data in **E** and **F** are expressed as means. (**G**) Cytokine concentrations in medium of BM macrophages before and after LPS stimulation (n = 4–6 per genotype, assayed in duplicate). *P < 0.05, ***P < 0.001 versus *Pggt1b*$^{fl/+}$*LC*.

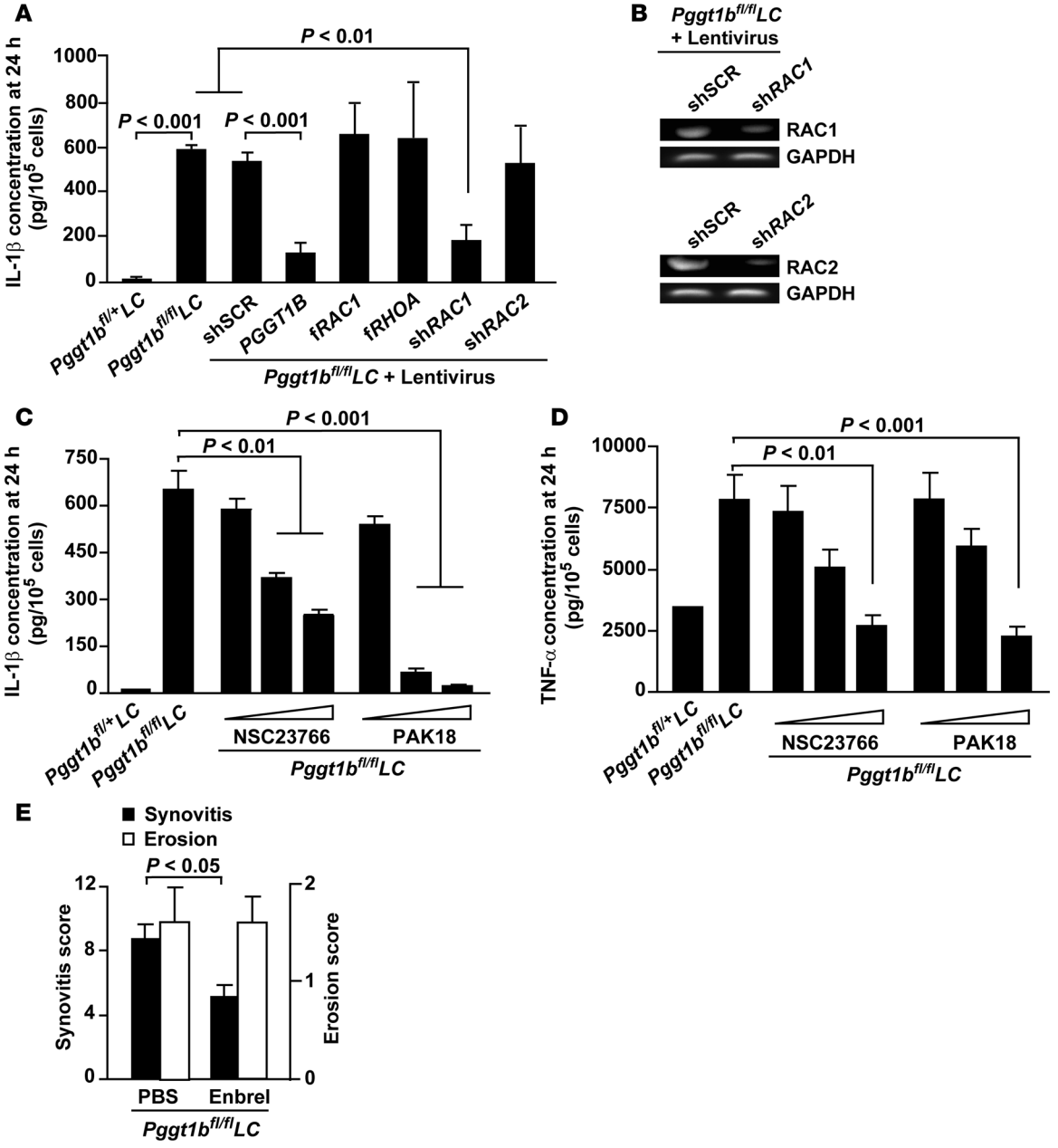

Figure 5

Inhibiting RAC1 reduces IL-1β and TNF-α secretion of *Pggt1b*$^{fl/fl}$*LC* BM macrophages, and TNF-α inhibition in vivo reduces joint inflammation. (**A**) Concentration of IL-1β in the medium of BM macrophages incubated with lentiviruses expressing the indicated constructs and then stimulated with LPS for 24 hours (n = 4–7 cell lines per treatment). shSCR, sequence-scrambled shRNA control. (**B**) Semiquantitative RT-PCR of cDNA from BM macrophages incubated with lentiviruses expressing the indicated constructs. Similar results were found with RT-QPCR analyses. (**C** and **D**) Concentration of IL-1β (**C**) and TNF-α (**D**) in medium of BM macrophages incubated with inhibitors of RAC1 (NSC23766; 10, 50, and 100 μM) and PAK (PAK18; 1, 5, and 10 μM) and stimulated with LPS for 24 hours (n = 3 cell lines per treatment). Data in **A**, **C**, and **D** are expressed as picogram cytokines normalized to 10^5 viable cells. (**E**) Synovitis and bone erosion in 20-week-old *Pggt1b*$^{fl/fl}$*LC* mice treated with vehicle (PBS, n = 11) or Enbrel (100 mg/kg/week, i.p., n = 9) for 8 weeks.

TNF-α is a well-known drug target in the treatment of rheumatoid arthritis. To determine whether TNF-α might be important for the disease phenotypes in vivo, we treated 12-week-old *Pggt1b*$^{fl/fl}$*LC* mice with the TNF-α receptor analog Enbrel (etanercept; Wyeth Pharmaceuticals) for 8 weeks. Synovitis was reduced by 41%; bone erosions were unaffected (Figure 5E).

Discussion

In this study, we tested the hypothesis that inactivating GGTase-I would reduce the development of inflammatory disorders in mice. Contrary to our expectations, inactivating GGTase-I in macrophages resulted in sustained activation of RHO proteins, increased the production of ROS and cytokines, and induced a severe inflam-

matory joint disease in vivo. The disease was chronic, progressive, and associated with synovitis, bone erosions, and increased serum levels of autoantibodies — phenotypes resembling rheumatoid arthritis in humans. The arthritis in *Pggt1b*$^{fl/fl}$*LC* mice was similar in outbred and inbred genetic strains, and synovitis and bone erosions were reversible in BM transplantation experiments.

Macrophages are important in the pathogenesis of rheumatoid arthritis (25–27). However, they are primarily viewed as effector cells that contribute to the progression rather than the initiation of rheumatoid arthritis (28, 29). Our results challenge that view and suggest that macrophages can initiate erosive arthritis in *Pggt1b*$^{fl/fl}$*LC* mice. First, the *LC* allele induced greater than 90% recombination of *Pggt1b* in macrophages, but only 40% in neutrophils, and little or no recombination in dendritic cells and lymphocytes. Second, GGTase-I–deficient macrophages were found at high levels in the synovium of *Pggt1b*$^{fl/fl}$*LC* mice. Third, GGTase-I–deficient macrophages showed exaggerated responses to inflammatory mediators in vitro. Fourth, monocyte depletion with etoposide reduced arthritis in *Pggt1b*$^{fl/fl}$*LC* mice. Cre recombination was also high in osteoclasts. However, we believe it unlikely that osteoclasts initiated the arthritis because infiltration of GGTase-I–deficient macrophages invariably preceded bone erosions in the joints, and overall bone health was unaffected.

Joint inflammation was reduced by Enbrel treatment, indicating that TNF-α drives arthritis in *Pggt1b*$^{fl/fl}$*LC* mice. GGTase-I–deficient macrophages secreted high levels of TNF-α in vitro, and macrophages are believed to be the main source of this cytokine in vivo (30). However, we cannot rule out the possibility that the action of TNF-α derived from other cell types, such as lymphocytes, is affected by Enbrel treatment. Enbrel treatment did not affect bone erosions, which suggests that TNF-α explains only part of the phenotype.

GGTase-I–deficient macrophages in culture had a reduced adhesive area, consistent with a role for RHO family proteins in regulating the cytoskeleton (2). The adhesive area was readily restored by expressing fRHOA or fRAC1. Thus, prenylation of RHOA and RAC1 appears to be required for their ability to regulate the spreading of macrophages in culture. Surprisingly, the absence of GGTase-I did not affect the ability of macrophages to migrate or phagocytose bacteria, which suggests that geranylgeranylation is dispensable for those processes.

GTP-bound forms of RAC1 and CDC42 were present at high levels in GGTase-I–deficient macrophages without corresponding increases in total protein levels. One potential explanation is that geranylgeranylation may be required for the binding of RHO family proteins to RHO-GAPs. In support of this reasoning, one study showed that RHO-GAPs cannot stimulate GTP hydrolysis of nonprenylated RHO proteins (10). Another potential explanation is that geranylgeranylation stimulates the interaction between RHO family proteins and RHO-GDI (4, 31, 32). Indeed, the association between RHO-GDI and RAC1 and between RHO-GDI and CDC42 was reduced in GGTase-I–deficient macrophages. In contrast, the association between RHO-GDI and RHOA was not affected by GGTase-I deficiency, which is consistent with previous studies (33, 34) and may explain the relatively low level of accumulation of GTP-bound RHOA compared with RAC1 and CDC42. A recent study provided a different perspective on the importance of RHO protein geranylgeranylation and the RHO-GDI interaction (35). Knockdown of RHO-GDI resulted in degradation of RHOA, RAC1, and CDC42. Interestingly, degradation only occurred if the proteins were geranylgeranylated. Thus, when RHO-GDI levels are limiting, the geranylgeranyl lipid targets the RHO proteins for degradation.

A substantial proportion of RAC1 in GGTase-I–deficient macrophages was localized at the plasma membrane; we found no evidence of nuclear localization. In contrast, several studies show that nonprenylated RAC1 is localized in the nucleus (6, 7, 32). These divergent results may relate to the use of different cell types and antibodies and to the fluorescent tags used to determine the subcellular localization of RAC1 in earlier studies. We used a specific antibody to locate endogenous RAC1 in GGTase-I–deficient macrophages by immunohistochemistry; the results were consistent with Western blots of subcellular fractions. RAC1 has a strong polybasic sequence (8), and electrostatic interactions may be sufficient for plasma membrane targeting.

Interestingly, trace amounts of RAC1 were present in the nuclear fraction of control *Pggt1b*$^{fl/+}$*LC* macrophages. This finding is consistent with a report of endogenous prenylated RAC1 in the nucleus of several cell types (32). Because no RAC1 was identified in the nuclei of *Pggt1b*$^{fl/fl}$*LC* macrophages, geranylgeranylation may be required for RAC1 nuclear import.

The observations that *Pggt1b*$^{fl/fl}$*LC* macrophages exhibited normal migration and phagocytosis and that RAC1 was found on the plasma membrane raise the question of whether GGTase-I substrates might be processed by FTase, residual GGTase-I activity, or RAB protein prenyltransferase GGTase-II. However, several results argue against that reasoning. First, GGTase-I substrates, including RAC1 and RHOA, accumulated in unprocessed form in *Pggt1b*$^{fl/fl}$*LC* macrophages. Second, RAC1 in *Pggt1b*$^{fl/fl}$*LC* macrophages exhibited reduced electrophoretic mobility. Third, RAC1 remained associated with the plasma membrane in GGTase-I–deficient macrophages incubated with an FTI and a GGTI.

The plasma membrane location and increased levels of RAC1-GTP can explain the LPS-induced increase in cytokine production by GGTase-I–deficient macrophages. IL-1β and TNF-α levels were reduced in cells treated with a *RAC1* shRNA lentivirus and with inhibitors of RAC1 and PAK. Interestingly, increased IL-1β secretion was observed in earlier studies, in which protein prenylation was reduced indirectly by a deficiency in mevalonate kinase or by statin treatment (36–38). However, the reduced isoprenoid synthesis in those studies likely affected both the farnesylation and the geranylgeranylation of *CAAX* proteins, as well as the geranylgeranylation of the RAB family proteins, which are prenylated by an unrelated enzyme, GGTase-II (39). Our results provide a firm link between nonprenylated RAC1 and increased cytokine production in macrophages.

In summary, inactivating GGTase-I in macrophages resulted in sustained activation of RHO family proteins and spontaneous erosive arthritis in mice. The results challenge the view that geranylgeranylation is essential for the activity and membrane targeting of RAC1 and other RHO family proteins, suggesting that one role of protein geranylgeranylation is to inhibit, rather than stimulate, their activity.

Methods

Gene-targeted mice, genotyping, and quantification of Cre recombination. Mice homozygous for a conditional knockout allele of the β subunit of GGTase-I and heterozygous for the lysozyme M–*Cre* knockin allele (*Pggt1b*$^{fl/fl}$*LC*) have been described previously (13). Controls were littermate *Pggt1b*$^{fl/+}$*LC* mice; additional controls were littermate *Pggt1b*$^{+/+}$*LC*, *Pggt1b*$^{fl/+}$, and *Pggt1b*$^{fl/fl}$

mice, collectively called wild-type. Genotyping and quantification of Cre recombination were done as described previously (13). Mice harboring *Fntb*^{fl}, a conditional knockout allele for the β subunit of FTase, were recently created (22). Mice were on a mixed genetic background (129Ola/Hsd-C57BL/6) or backcrossed 5 times onto a pure C57BL/6 background. Mouse experiments were approved by the University of Gothenburg Animal Research Ethics Committee.

Generation of BM-derived and peritoneal macrophages. BM cells were harvested from femur and tibia and plated in high-glucose DMEM supplemented with 10% fetal calf serum, 1% HEPES, 1% glutamine, 1% gentamicin, 0.01% β-mercaptoethanol, and 10% whole supernatant of cell line CMG14-12 as a source of mouse M-CSF (40). Experiments were performed on differentiated macrophages on days 7–10 after plating. i.p. macrophages were collected 4 days after an i.p. injection of 2 ml of 3% uric acid (41). Experiments were performed on days 1–3 after plating. Experiments were performed at least twice with macrophages prepared on different days.

Generation of osteoclasts and isolation of myeloid subsets and lymphocytes. Osteoclasts were generated by incubating BM-derived macrophages with 40 ng/ml recombinant RANK ligand (Invitrogen) for 5 days as described previously (42); identity of osteoclasts was confirmed by staining for tartrate-resistant acid phosphatase (TRAP Staining Kit, Sigma-Aldrich). Dendritic cells were isolated from spleens with the Dendritic Cell Enrichment Kit (Invitrogen). Neutrophils were isolated from peripheral blood as described previously (43). CD3$^+$ lymphocytes were isolated from spleens by FACS sorting.

Histology and immunohistochemistry. For routine histology, joints were decalcified in Parengy buffer and fixed in 4% paraformaldehyde, embedded in paraffin, sectioned, and stained with hematoxylin and eosin. For immunohistochemistry, joints were decalcified in 0.1 M Tris-EDTA buffer and frozen in OCT (Sakura Finetek). Cryosections were incubated with antibodies recognizing F4/80 (catalog no. MCA-497, Serotec), np-RAP1A (catalog no. sc-1482, Santa Cruz Biotechnology), and CD4 (catalog no. 550280, BD Biosciences — Pharmingen) overnight at 4°C and with biotinylated anti-goat or anti-rat secondary antibodies (Vector Laboratories) for 1 h at room temperature. The slides were then incubated with StreptABComplxes (Dako) and hydrogen peroxide and counterstained with Mayer hematoxylin. Slides were analyzed with a Zeiss Axioplan 2 microscope (Carl Zeiss AG).

Quantifying inflammation and bone erosion in mouse joints. Synovitis and bone erosion were evaluated in the knee, ankle, metatarsal, elbow, wrist, and metacarpal joints of mice by an observer blinded to genotype. Synovitis was defined as a synovial membrane thickness of more than 2 cell layers. Synovitis and subchondral bone erosion in each joint were individually scored as 1 (mild), 2 (moderate), or 3 (severe), and the scores were added to produce total inflammation and erosion scores for each mouse (44).

Etoposide and Enbrel treatment. For monocyte depletion, etoposide (10 mg/kg; Bristol-Myers Squibb) was injected subcutaneously in 4-week-old mice every second day for 8 weeks (24). To inhibit TNF-α signaling in vivo, Enbrel (TNF-α receptor analog; 100 mg/kg/week; Wyeth Pharmaceuticals) was injected i.p. in 6- to 8-week-old mice every second day for 8 weeks (45). Littermate controls were injected with PBS.

Measurement of serum antibodies. Antibodies recognizing CCP, Fc-IgG (RF), ssDNA, and collagen type II were measured in serum from 12-week-old mice as described previously (46–48).

BM transplantation. BM cells were harvested from femur and tibia of donor mice. Recipient mice were given neomycin and polymyxin-B in the drinking water for 7 days (to prevent radiation damage–induced infections) before and after a lethal dose of radiation (950 Gy). The day after irradiation, mice were injected with 10^7 unfractionated donor cells in 200 μl RPMI-1640 as described previously (49). Engraftment was confirmed by genotyping genomic DNA from peripheral blood of the recipient mice.

FACS analyses. BM macrophages were incubated with antibodies recognizing CD45 (catalog no. 557659), CD11b (catalog no. 550993), CD11c (catalog no. 550261), MAC3 (catalog no. 553324), Gr-1 (catalog no. 553129, BD Biosciences), MAC2 (catalog no. 8942F; Cederlane), and F4/80 (catalog no. MCA497APC; Serotec) and analyzed in a FACSAria Flow Cytometer (BD Biosciences). Data were analyzed with FACSDiva software (version 6.1.1; BD Biosciences). Apoptosis was detected with the Annexin V:EGFP Apoptosis Detection Kit (Biovision).

Immunoprecipitation, subcellular fractionation, and Western blotting. Total cellular lysates were isolated as described previously (50). GTP-bound RAC1 and CDC42 were affinity precipitated with PAK1-GST (EZ Detect Rac1 Activation Kit; Pierce), and GTP-bound RHOA was affinity precipitated with RHOTEKIN-GST (RhoA Activation Biochem Kit; Cytoskeleton). Immunoprecipitation of RHO-GDI was performed with a monoclonal antibody (catalog no. sc-360, Santa Cruz Biotechnology) and the Dynabeads Protein G immunoprecipitation kit (catalog no. 100-07D, Invitrogen). For analyses of p38 activation, lysates were prepared from BM macrophages before and 15 minutes after stimulation with LPS (10 ng/ml); for NF-κB activation, lysates were isolated before and 15 and 30 minutes after stimulation. Isolation of subcellular fractions was done with the Qproteome Cell Compartment Kit (Qiagen). Protein samples were run on 10%–20%, 12%, or 18% SDS-PAGE gels (Criterion, Protean, BioRad), transferred to nitrocellulose or PVDF membranes, and incubated with antibodies to RAC1 (catalog no. 05-389, Millipore; and antibody supplied in RAC1 activation kit, Pierce), RHOA (catalog no. ARH03-B, Cytoskeleton), CDC42 (catalog no. sc-2462), np-RAP1A (catalog no. sc-1482), RHO-GDIα (catalog no. sc-360), lamin A/C (catalog no. sc-7293, Santa Cruz Biotechnology), $β_1$-integrin (catalog no. 4706), phospho-p38 (catalog no. 9211), total p38 (catalog no. 9212), phospho-p65^{Ser536} (catalog no. 3031, Cell Signaling), FLAG-tag (catalog no. F3165, Sigma-Aldrich), MYC-tag (catalog no. R950-25, Invitrogen), and actin (catalog no. A2066, Sigma-Aldrich). Prelamin A antibody was provided by S.G. Young and L.G. Fong (UCLA, Los Angeles, California, USA). Protein bands were visualized with horseradish peroxidase–conjugated secondary antibodies (catalog no. sc-2354, Santa Cruz Biotechnology; catalog nos. NA931 and NA934, GE Healthcare) and the ECL Western blotting system (GE Healthcare). Protein bands were analyzed by densitometry with Quantity One (version 4.4.0; Bio-Rad).

Phalloidin staining and immunocytochemistry. Macrophages on chamber slides were fixed with 4% paraformaldehyde for 15 minutes, permeabilized in 0.1 % Triton X-100 for 5 minutes, and stained with Alexa Fluor 647–labeled phalloidin (catalog no. A22287, Invitrogen) for 20 minutes. For immunocytochemistry, macrophages were fixed with ice-cold methanol, permeabilized in 1.0% Triton X-100 for 15 minutes, and incubated with antibodies recognizing RAC1 (catalog no. ARC03, Cytoskeleton) and Na/K-ATPase-α (catalog no. 28800, Santa Cruz Biotechnology) overnight at 4°C. The slides were then incubated with Alexa Fluor 488– and 547–labeled secondary antibodies (catalog nos. A11001 and A10040, respectively, Invitrogen) for 1 hour, mounted with Prolong Antifade with DAPI (catalog no. P36935, Invitrogen), and analyzed with a Leica TCS SP5 confocal microscope and LAS Advanced Fluorescence software (version 2.0.2, Leica Microsystems).

Lentivirus experiments. A FLAG-tagged fRAC1 construct (RAC1-CVLS) was generated by PCR amplification of mouse cDNA with forward primer 5′-AGGATCCGAAATGGACTACAAGGACGACGATGACAAGATGCAGGCCATCAAGTGTGTGGTGG-3′ and reverse primer 5′-AGGATCCTTACGAGAGCACGCATTTTCTCTTCCTCTTC-3′. A MYC-tagged fRHOA construct (RHOA-CVLS) was generated as described previously (13). The human PGGT1B cDNA clone was from Imagenes (catalog no. EX-C0587). fRAC1, fRHOA, and PGGT1B constructs were cloned into lentiviral vector pCD521A-1_pCHD-EF1dTomato-T2A (catalog no. CD520A-1, Biocat). Lentiviruses expressing RAC1 and RAC2 shRNA were from

Sigma-Aldrich (accession nos. NM_009007 and NM_009008, respectively). BM macrophages were incubated with lentiviruses (5–20 MOI) for 2 days before experiments.

Migration and phagocytosis. Migration of BM and i.p. macrophages in response to D-peptide (hexapeptide, WKYMVM) was evaluated with a modified Boyden chamber assay as described previously (41, 51). For analysis of phagocytosis, 2×10^5 macrophages were incubated with 3×10^6 bacteria (*Staphylococcus aureus*, LS-1) for 50 minutes. After 3 washes in PBS, the macrophages were lysed in sterile water, and serial dilutions were plated onto blood agar plates and incubated overnight at 37°C. Phagocytosis was reported as CFU per milliliter lysed macrophage suspension (52).

In vitro prenylation assay to assess accumulation of GGTase-I substrates. BM-derived macrophages were resuspended in a buffer containing 50 mM Tris-HCl, 1 M $MgCl_2$, 10 mM DTT, 1 mM PMSF, 2.5 mM NaF, and 1 mM Na_2VO_3; sonicated; and centrifuged at 21,000 *g* for 20 minutes. Supernatants (600 μg) were incubated with 50 ng recombinant human GGTase-I (provided by P.J. Casey, Duke University Medical Center, Durham, North Carolina, USA; ref. 53) and 6 μCi ^{3}H-GGPP (American Radiolabeled Chemicals Inc.) for 1 hour at 30°C. Total proteins were precipitated with acetone; alternatively, RAC1 and RHOA were immunoprecipitated from the reaction mixture as described above. Proteins were resolved on 12% Tris-HCl Criterion gels (Biorad); the gel was incubated with Autofluor (National Diagnostics), dried, and exposed to X-ray film for 3–28 days.

Assays for ROS and NF-κB activity. BM macrophages (5×10^5) were incubated with isoluminol (56 μM) and horseradish peroxidase (4 U) and stimulated with 50 μM PMA (Sigma-Aldrich). Total extracellular ROS production was estimated by integrating area-under-the-curve data from real-time chemiluminescence measurements (Bio-Orbit 1251 Luminometer, Thermo Labsystems; ref. 54). NF-κB p65 activity was measured in total cellular lysates of BM macrophages stimulated with LPS for 15 and 30 minutes with the TransAM NF-κB p65 transcription factor ELISA kit (catalog no. 40096, Active Motif).

Gene expression analyses on low-density arrays. RNA was isolated from BM and i.p. macrophages with the RNeasy Mini Kit (Qiagen) before and 12 hours after LPS stimulation. cDNA was synthesized with the RT^2 First Strand Kit (C-03, SuperArray, SABiosciences), and gene expression was analyzed with the mouse NF-κB Signaling Pathway PCR Array (catalog no. PAMM-025C, SABiosciences) and the Extracellular Matrix and Adhesion Molecules PCR Array (catalog no. PAMM-013C, SABiosciences). Genes with statistically significant changes in expression were confirmed individually with TaqMan RT-QPCR using different primers.

Cytokine analyses. BM macrophages (10^5 cells) were cultured overnight in medium without M-CSF, then stimulated with 10 ng/ml LPS in fresh medium. In some experiments, cells were incubated with lentiviruses expressing fRAC1, fRAC2, PGGT1B, shRAC1, and shRAC2 and inhibitors of RAC1 (NSC23766, Merck) and PAK (PAK18, Merck) for 2 days before stimulation. After stimulation, the medium was harvested, and viable cells were counted (duplicate wells per cell line per time point). Concentrations of cytokines were measured in the medium with the Mouse ProInflammatory 7-plexUltrasensitive Kit in a SECTOR 2400 Imager (Meso Scale Discovery). IL-1β and TNF-α were also analyzed by ELISA (catalog nos. 88-7013-22 and 88-7324-22, respectively, BD Biosciences).

Statistics. Values are mean ± SEM unless otherwise indicated. Differences between groups were determined with 2-tailed *t* test or 1-way ANOVA; a *P* value less than 0.05 was considered significant.

Acknowledgments

This study was supported by a Starting Investigator Grant from the European Research Council; by grants from the Swedish Cancer Society, the Swedish Medical Research Council, the Swedish Children's Cancer Fund, and Västra Götalandsregionen (to M.O. Bergo); and by the Swedish Foundation for Strategic Research (to O.M. Khan, M. Bokarewa, and M.O. Bergo). We thank Stephen Ordway for editing the manuscript, Stephen Young and Loren Fong for the prelamin A antibody and helpful discussions, Patrick Casey for recombinant GGTase-I, Huamei Forsman for neutrophil preparations, Anette Hansevi for CT scans, and the late Andrej Tarkowski for his great contribution to this work.

Received for publication May 19, 2010, and accepted in revised form November 10, 2010.

Address correspondence to: Martin Bergo, Wallenberg Laboratory, Bruna Straket 16, 3rd floor, Sahlgrenska University Hospital, S-413 45 Gothenburg, Sweden. Phone: 46.31.342.78.58; Fax: 46.31.82.37.62; E-mail: martin.bergo@wlab.gu.se.

1. Hall A. G proteins and small GTPases: distant relatives keep in touch. *Science*. 1998;280(5372):2074–2075.
2. Heasman SJ, Ridley AJ. Mammalian Rho GTPases: new insights into their functions from in vivo studies. *Nat Rev Mol Cell Biol*. 2008;9(9):690–701.
3. Zhang FL, Casey PJ. Influence of metal ions on substrate binding and catalytic activity of mammalian protein geranylgeranyltransferase type-I. *Biochem J*. 1996;320(pt 3):925–932.
4. Hori Y, et al. Post-translational modifications of the C-terminal region of the rho protein are important for its interaction with membranes and the stimulatory and inhibitory GDP/GTP exchange proteins. *Oncogene*. 1991;6(4):515–522.
5. Solski PA, Helms W, Keely PJ, Su LS, Der CJ. RhoA biological activity is dependent on prenylation but independent of specific isoprenoid modification. *Cell Growth Differ*. 2002;13(8):363–373.
6. Yoshizaki H, et al. Activity of Rho-family GTPases during cell division as visualized with FRET-based probes. *J Cell Biol*. 2003;162(2):223–232.
7. Wong KW, Isberg RR. Yersinia pseudotuberculosis spatially controls activation and misregulation of host cell Rac1. *PLoS Pathog*. 2005;1(2):e16.
8. Michaelson D, Silletti J, Murphy G, D'Eustachio P, Rush M, Philips MR. Differential localization of Rho GTPases in live cells: regulation by hypervariable regions and RhoGDI binding. *J Cell Biol*. 2001;152(1):111–126.
9. Sasaki T, Kato M, Takai Y. Consequences of weak interaction of Rho GDI with the GTP-bound forms of Rho p21 and Rac p21. *J Biol Chem*. 1993; 268(32):23959–23963.
10. Molnar G, Dagher MC, Geiszt M, Settleman J, Ligeti E. Role of prenylation in the interaction of Rho-family small GTPases with GTPase activating proteins. *Biochemistry*. 2001;40(35):10542–10549.
11. Turner SJ, Zhuang S, Zhang T, Boss GR, Pilz RB. Effects of lovastatin on RHO isoform expression, activity, and association with guanine nucleotide dissociation inhibitors. *Biochem Pharmacol*. 2008; 75(2):405–413.
12. Sahai E, Marshall CJ. RHO-GTPases and cancer. *Nat Rev Cancer*. 2002;2(2):133–142.
13. Sjogren AKM, et al. GGTase-I deficiency reduces tumor formation and improves survival in mice with K-RAS-induced lung cancer. *J Clin Invest*. 2007; 117(5):1294–1304.
14. Connor AM, Berger S, Narendran A, Keystone EC. Inhibition of protein geranylgeranylation induces apoptosis in synovial fibroblasts. *Arthritis Res Ther*. 2006;8(4):R94.
15. Nagashima T, Okazaki H, Yudoh K, Matsuno H, Minota S. Apoptosis of rheumatoid synovial cells by statins through the blocking of protein geranylgeranylation: a potential therapeutic approach to rheumatoid arthritis. *Arthritis Rheum*. 2006;54(2):579–586.
16. Jain MK, Ridker PM. Anti-inflammatory effects of statins: Clinical evidence and basic mechanisms. *Nat Rev Drug Discov*. 2005;4(12):977–987.
17. Greenwood J, Steinman L, Zamvil SS. Statin therapy and autoimmune disease: from protein prenylation to immunomodulation. *Nat Rev Immunol*. 2006;6(5):358–370.
18. Kanda H, et al. Antiinflammatory effect of simvastatin in patients with rheumatoid arthritis. *J Rheumatol*. 2002;29(9):2024–2026.
19. McCarey DW, et al. Trial of Atorvastatin in Rheumatoid Arthritis (TARA): double-blind, randomised placebo-controlled trial. *Lancet*. 2004; 363(9426):2015–2021.
20. Paraskevas KI. Statin treatment for rheumatoid arthritis: a promising novel indication. *Clin Rheumatol*. 2008;27(3):281–287.
21. Winter-Vann AM, Casey PJ. Opinion – Post-prenylation-processing enzymes as new targets in oncogenesis. *Nat Rev Cancer*. 2005;5(5):405–412.
22. Liu M, et al. Targeting the protein prenyltransferases efficiently reduces tumor development in mice with K-RAS-induced lung cancer. *Proc Natl Acad Sci U S A*.

2010;107(14):6471–6476.
23. Vantwout JW, Linde I, Leijh PCJ, Vanfurth R. Effect of irradiation, cyclophosphamide, and etoposide (Vp-16) on number of peripheral-blood and peritoneal leukocytes in mice under normal conditions and during acute inflammatory reaction. *Inflammation*. 1989;13(1):1–14.
24. Verdrengh M, Tarkowski A. Role of macrophages in Staphylococcus aureus-induced arthritis and sepsis. *Arthritis Rheum*. 2000;43(10):2276–2282.
25. Drexler SK, Kong PL, Wales J, Foxwell BM. Cell signalling in macrophages, the principal innate immune effector cells of rheumatoid arthritis. *Arthritis Res Ther*. 2008;10(5):216.
26. Tak PP, et al. Analysis of the synovial cell infiltrate in early rheumatoid synovial tissue in relation to local disease activity. *Arthritis Rheum*. 1997; 40(2):217–225.
27. Bondeson J. The mechanisms of action of disease-modifying antirheumatic drugs: A review with emphasis on macrophage signal transduction and the induction of proinflammatory cytokines. *Gen Pharmacol*. 1997;29(2):127–150.
28. Cope AP, Schulze-Koops H, Aringer M. The central role of T cells in rheumatoid arthritis. *Clin Exp Rheumatol*. 2007;25(5 suppl 46):S4–S11.
29. Goronzy JJ, Weyand CM. T-cell regulation in rheumatoid arthritis. *Curr Opin Rheumatol*. 2004; 16(3):212–217.
30. Beutler B, Cerami A. Cachectin: more than a tumor necrosis factor. *N Engl J Med*. 1987;316(7):379–385.
31. Olofsson B. Rho guanine dissociation inhibitors: Pivotal molecules in cellular signalling. *Cell Signal*. 1999;11(8):545–554.
32. Michaelson D, et al. RAC1 accumulates in the nucleus during the G2 phase of the cell cycle and promotes cell division. *J Cell Biol*. 2008;181(3):485–496.
33. Faure J, Dagher MC. Interactions between RHO GTPases and RHO GDP dissociation inhibitor (Rho-GDI). *Biochimie*. 2001;83(5):409–414.
34. Rolli-Derkinderen M, et al. Phosphorylation of serine 188 protects RHOA from ubiquitin/proteasome-mediated degradation in vascular smooth muscle cells. *Circ Res*. 2005;96(11):1152–1160.
35. Boulter E, et al. Regulation of RHO GTPase crosstalk, degradation and activity by RHOGDI1. *Nat Cell Biol*. 2010;12(5):477–483.
36. Lindholm MW, Nilsson J. Simvastatin stimulates macrophage interleukin-1beta secretion through an isoprenylation-dependent mechanism. *Vascul Pharmacol*. 2007;46(2):91–96.
37. Mandey SH, Kuijk LM, Frenkel J, Waterham HR. A role for geranylgeranylation in interleukin-1beta secretion. *Arthritis Rheum*. 2006;54(11):3690–3695.
38. Kuijk LM, Beekman JM, Koster J, Waterham HR, Frenkel J, Coffer PJ. HMG-CoA reductase inhibition induces IL-1β release through RAC1/PI3K/PKB-dependent caspase-1 activation. *Blood*. 2008;112(9):3563–3573.
39. Leung KF, Baron R, Seabra MC. Geranylgeranylation of RAB GTPases. *J Lipid Res*. 2006;47(3):467–475.
40. Takeshita S, Kaji K, Kudo A. Identification and characterization of the new osteoclast progenitor with macrophage phenotypes being able to differentiate into mature osteoclasts. *J Bone Miner Res*. 2000; 15(8):1477–1488.
41. Zare F, et al. Uric acid, a nucleic acid degradation product, down-regulates dsRNA-triggered arthritis. *J Leukoc Biol*. 2006;79(3):482–488.
42. Lacey DL, et al. Osteoprotegerin ligand is a cytokine that regulates osteoclast differentiation and activation. *Cell*. 1998;93(2):165–176.
43. Itou T, Collins LV, Thoren FB, Dahlgren C, Karlsson A. Changes in activation states of murine polymorphonuclear leukocytes (PMN) during inflammation: a comparison of bone marrow and peritoneal exudate PMN. *Clin Vaccine Immunol*. 2006; 13(5):575–583.
44. Verdrengh M, Tarkowski A. The impact of substance P signalling on the development of experimental staphylococcal sepsis and arthritis. *Scand J Immunol*. 2008;67(3):253–259.
45. Bokarewa M, Nagaev I, Dahlberg L, Smith U, Tarkowski A. Resistin, an adipokine with potent proinflammatory properties. *J Immunol*. 2005; 174(9):5789–5795.
46. Lindblad SS, Mydel P, Jonsson IM, Senior RM, Tarkowski A, Bokarewa M. Smoking and nicotine exposure delay development of collagen–induced arthritis in mice. *Arthritis Res Ther*. 2009;11(3):R88.
47. Verdrengh M, Jonsson IM, Holmdahl R, Tarkowski A. Genistein as an anti-inflammatory agent. *Inflamm Res*. 2003;52(8):341–346.
48. Zhao Y, Tozawa Y, Iseki R, Mukai M, Iwata M. Calcineurin Activation Protects T-Cells from Glucocorticoid-Induced Apoptosis. *J Immunol*. 1995; 154(12):6346–6354.
49. Cutts BA, et al. Nf1 deficiency cooperates with oncogenic K-RAS to induce acute myeloid leukemia in mice. *Blood*. 2009;114(17):3629–3632.
50. Bergo MO, et al. Inactivation of Icmt inhibits transformation by oncogenic K-Ras and B-Raf. *J Clin Invest*. 2004;113(4):539–550.
51. Pullerits R, Brisslert M, Jonsson IM, Tarkowski A. Soluble receptor for advanced glycation end products triggers a proinflammatory cytokine cascade via b2 integrin Mac-1. *Arthritis Rheum*. 2006;54(12):3898–3907.
52. Jonsson IM, Lindholm C, Luong TT, Lee CY, Tarkowski A. mgrA regulates staphylococcal virulence important for induction and progression of septic arthritis and sepsis. *Microbes Infect*. 2008; 10(12–13):1229–1235.
53. Moomaw JF, Zhang FL, Casey PJ. Isolation of protein prenyltransferases from bovine brain and baculovirus expression system. *Methods Enzymol*. 1995;250:12–21.
54. Hulten LM, Holmstrom M, Soussi B. Harmful singlet oxygen can be helpful. *Free Radic Biol Med*. 1999;27(11–12):1203–1207.